Contributions of Anthropogenic and Natural Forcing to Recent Tropopause Height Changes

B. D. Santer,[1]* M. F. Wehner,[2] T. M. L. Wigley,[3] R. Sausen,[4] G. A. Meehl,[3] K. E. Taylor,[1] C. Ammann,[3] J. Arblaster,[3] W. M. Washington,[3] J. S. Boyle,[1] W. Brüggemann[5]

Observations indicate that the height of the tropopause—the boundary between the stratosphere and troposphere—has increased by several hundred meters since 1979. Comparable increases are evident in climate model experiments. The latter show that human-induced changes in ozone and well-mixed greenhouse gases account for ~80% of the simulated rise in tropopause height over 1979–1999. Their primary contributions are through cooling of the stratosphere (caused by ozone) and warming of the troposphere (caused by well-mixed greenhouse gases). A model-predicted fingerprint of tropopause height changes is statistically detectable in two different observational ("reanalysis") data sets. This positive detection result allows us to attribute overall tropopause height changes to a combination of anthropogenic and natural external forcings, with the anthropogenic component predominating.

The tropopause represents the boundary between the troposphere and stratosphere and is marked by large changes in the thermal, dynamical, and chemical structure of the atmosphere (*1*–*3*). Increases in tropopause height over the past several decades have been identified in radiosonde data (*2*, *4*), in optimal combinations of numerical weather forecasts and observations ("reanalyses") (*3*, *5*), and in climate models forced by combined natural and anthropogenic effects (*6*). Model experiments suggest that such increases cannot be explained by natural climate variability alone (*6*, *7*).

To date, no study has quantified the contributions of different anthropogenic and natural forcings to 20th-century tropopause height changes. We estimate these contributions here and demonstrate the usefulness of the thermally defined tropopause as an integrated indicator of human-induced climate change. We also identify a model-predicted "fingerprint" of tropopause height changes in reanalysis data. Detection of this fingerprint enables us to attribute tropopause height changes to the combined effects of anthropogenic and natural forcing.

[1]Program for Climate Model Diagnosis and Intercomparison, Lawrence Livermore National Laboratory, Livermore, CA 94550, USA. [2]Lawrence Berkeley National Laboratory, Berkeley, CA 94720, USA. [3]National Center for Atmospheric Research, Boulder, CO 80303, USA. [4]Deutsches Zentrum für Luft- und Raumfahrt, Institut für Physik der Atmosphäre, Oberpfaffenhofen, D-82234 Wessling, Germany. [5]University of Birmingham, Edgbaston, Birmingham B15 2TT, UK.

*To whom correspondence should be addressed. E-mail: santer1@llnl.gov

The anthropogenic forcings we consider are changes in well-mixed greenhouse gases (G), the direct scattering effects of sulfate aerosols (A), and tropospheric and stratospheric ozone (O). The natural forcings considered are changes in solar irradiance (S) and volcanic aerosols (V). All of these factors are likely to have modified the thermal structure and static stability of the atmosphere (*6*–*11*), thus affecting tropopause height. To isolate the thermal responses that drive tropopause height changes, we analyze the effects of G, A, O, S, and V on temperatures averaged over broad layers of the stratosphere and troposphere.

Model and reanalysis data. We used the Department of Energy Parallel Climate Model (PCM) developed by the National Center for Atmospheric Research (NCAR) and Los Alamos National Laboratory (*12*). A wide range of experiments has been performed with PCM, of which seven were analyzed here for tropopause height changes. In the first five experiments, only a single forcing is changed at a time; for example, G varies according to historical estimates of greenhouse gas concentration changes, whereas A, O, S, and V are all held constant at preindustrial levels (*13*–*18*). In the sixth experiment (ALL), all five forcings are varied simultaneously. Both natural forcings are changed in the seventh experiment (SV). G, A, O, and S commence in 1872, whereas V, SV, and ALL start in 1890. The experiments end in 1999. To obtain better estimates of the underlying responses to the imposed forcings, four realizations of each experiment were performed. Each realization of a given experiment has identical forcing but commences from different initial conditions of an unforced control run.

The detection part of our study requires estimates of observed tropopause height changes, which were obtained from two reanalyses (*19*, *20*). The first is from the National Center for Environmental Prediction and the National Center for Atmospheric Research (NCEP); the second is from the European Centre for Medium-Range Weather Forecasts (ERA). Reanalyses use an atmospheric numerical weather forecast model with no changes over time in either the model itself or in the observational data assimilation system. NCEP data were available from 1948 to 2001, but data before January 1979 were excluded because of well-documented inhomogeneities (*21*, *22*). ERA spans the shorter period from 1979 to 1993.

We estimate tropopause height using a standard thermal definition of p_{LRT}, the pressure of the lapse-rate tropopause (*23*). This definition has the advantage that it can be applied globally and is easily calculated from vertical profiles of atmospheric temperature under most meteorological conditions (*24*, *25*). The algorithm that we used to compute p_{LRT} primarily monitors large-scale changes in the thermal structure of the atmosphere.

Multidecadal changes in p_{LRT} are generally smaller than the vertical resolution of the atmospheric models used in PCM and the two reanalyses (Fig. 1A). This raises concerns regarding the sensitivity of our estimated p_{LRT} trends to the vertical resolution of the input temperature data in the vicinity of the tropopause. Three independent pieces of evidence support the reliability of our p_{LRT} changes. First, calculations of NCEP p_{LRT} trends performed at high and low vertical resolution are in close agreement (*26*). Second, climate models with different vertical resolutions yield similar p_{LRT} trends in response to external forcing (*6*). Finally, p_{LRT} trends computed from ERA and NCEP are in good agreement with p_{LRT} changes obtained from high-resolution radiosonde temperature soundings (*4*, *6*). All three lines of evidence enhance confidence in the robustness of our procedure for estimating p_{LRT} changes.

At each grid point in the model and reanalysis data, we compute p_{LRT} from the monthly mean temperature profile at discrete pressure levels (*25*). For PCM, we also calculate stratospheric and tropospheric temperatures equivalent to those monitored by channels 4 and 2 (T4 and T2) of the satellite-based Microwave Sounding Unit (MSU) (*22*, *27*–*29*). The simulated MSU data are useful in relating changes in p_{LRT} to broad changes in atmospheric thermal structure. Direct comparisons with observed MSU T4 and T2 data are given elsewhere (*30*).

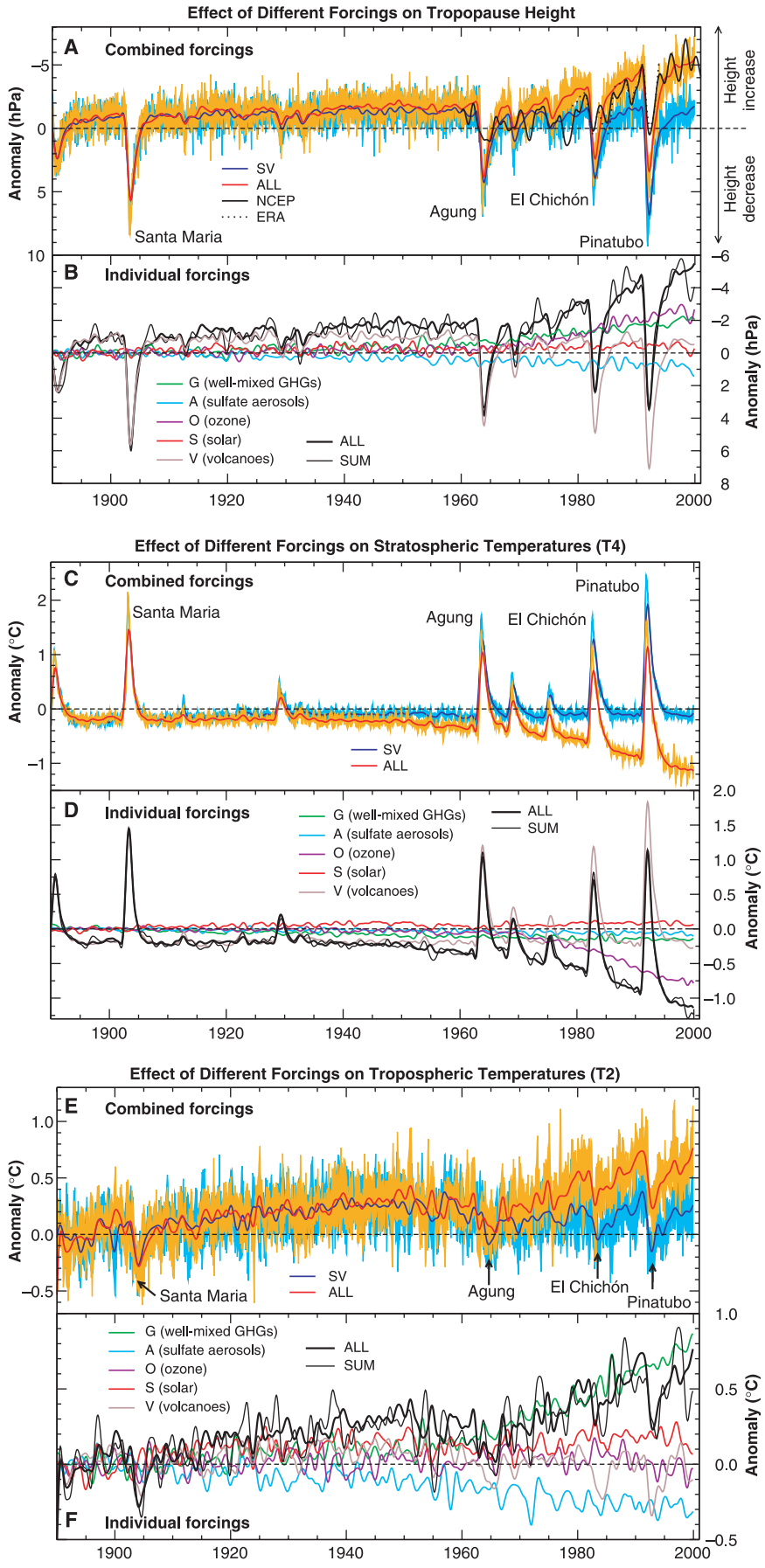

Fig. 1. Time series of global mean, monthly mean anomalies in tropopause pressure (p_{LRT})(**A** and **B**), stratospheric temperature (T4) (**C** and **D**), and mid- to upper tropospheric temperature (T2) (**E** and **F**). Model results are from seven different PCM ensemble experiments (*12*, *14*, *16*, *17*). Five experiments use a single forcing only (G, A, O, S, or V). Two integrations involve combined forcing changes, either in natural forcings (SV), or in all forcings (ALL). There are four realizations of each experiment. In (B), (D), and (F), only low-pass filtered ensemble means are shown. In (A), (C), and (E), both the low-pass filtered ensemble mean and the (unfiltered) range between the highest and lowest values of the realizations are given. All model anomalies are defined relative to climatological monthly means computed over 1890–1909. Reanalysis-based p_{LRT} estimates from NCEP (*19*) and ERA (*20*) were filtered in the same way as model data (A). NCEP p_{LRT} data are available from 1948–2001, but pre-1960 data were ignored because of deficiencies in the coverage and quality of assimilated radiosonde data (*22*). The ERA record spans 1979–1993. NCEP (ERA) was forced to have the same mean as ALL over 1960–1999 (1979–1993). The SUM results [(B), (D), and (F)] are the sum of the filtered ensemble-mean responses from G, A, O, S, and V.

Global-scale changes. For any specified forcing, the ensemble members define an envelope of possible climate trajectories (Fig. 1A). The time at which the ALL and SV envelopes separate completely (and remain separated) is a simple qualitative measure of the detectability of an anthropogenic signal in PCM data. For tropopause height, this separation occurs in the mid-1980s. Divergence of the ALL and SV solutions occurs earlier for T4 data [before the eruption of Mt. Agung in 1963 (Fig. 1C)] and later for T2 [in the early 1990s (Fig. 1E)].

The short-term (3- to 4-year) p_{LRT} signatures of major volcanic eruptions are clearly evident in reanalyses and the SV and ALL experiments (Fig. 1A). Large explosive volcanic eruptions warm the lower stratosphere and cool the troposphere (Fig. 1, C and E). Both effects decrease tropopause height and increase p_{LRT} (*6*). In PCM, p_{LRT} changes after the eruptions of Santa Maria, Agung, El Chichón, and Pinatubo are large, relative to both the "between realization" variability of p_{LRT} and the p_{LRT} variability during volcanically quiescent periods.

The total linear p_{LRT} decrease in ALL is 2.9 hPa over 1979–1999, corresponding to a tropopause height increase of roughly 120 m (Fig. 1A). Tropopause height in NCEP rises by ~190 m. The smaller increase in PCM is primarily due to two factors. The first is the unrealistically large stratospheric cooling in NCEP (*31*). Because stratospheric cooling tends to increase tropopause height (*4*, *6*), excessive cooling amplifies NCEP's height increase. The second factor is PCM's overestimate of volcanically induced stratospheric warming (*30*). Excessive stratospheric warming yields a volcanically induced tropopause height decrease that is too large, thus reducing the overall height increase in ALL.

The largest contributions to PCM's overall tropopause height increases are from changes in

well-mixed greenhouse gases and ozone (Fig. 1B). To quantify these contributions, we examine the total linear p_{LRT} trends in the ensemble means of the G, A, O, S, and V experiments (*32*). Linear trends are computed over four different time horizons: the 20th century, 1900–1949, 1950–1999, and the satellite era (1979–1999) (Fig. 2A). Contributions of individual forcings are expressed as a percentage of the total linear change in ALL (*33*). Because some forcings increase tropopause height and others lower it, the contributions of individual forcings can in some cases exceed 100%. This simply means that in the absence of other influences, the trend due to a specific forcing can be larger than that obtained when all five forcings act in concert.

During the 20th century, G and O account for 77 and 88% (respectively) of the total increase in tropopause height in ALL. Their combined percentage contribution of 165% is partly offset by the smaller decreases in height caused by A and V (−32 and −39%). Solar irradiance changes make a small positive contribution to the height increase in ALL. The relative contribution of each forcing varies with time. Whereas G and O make roughly equivalent contributions to tropopause height change over 1900–1949, ozone becomes more important in the second half of the century and during the satellite era (Fig. 2A). Similarly, S and V together explain 74% of the total tropopause height change over 1900–1949, but their net contribution to ALL is only −40% over 1950–1999. The large influence of V over 1900–1949 arises from the Santa Maria eruption in 1902 (Fig. 1A).

Decadal-scale increases in the height of the tropopause are driven by temperature changes above and below the tropopause. Temperatures in this region are influenced primarily by ozone- and greenhouse gas–induced cooling of the stratosphere and greenhouse gas–induced warming of the troposphere. Both of these effects tend to raise tropopause height (*4*, *6*). To first order, the global mean changes in p_{LRT} over a stipulated time period are linearly related to ΔT4 − ΔT2. A key question, therefore, is whether the simulated height increase in ALL could have occurred solely through stratospheric cooling and without significant anthropogenically induced warming of the troposphere. We address this question by estimating the contributions of individual forcings to T4 and T2 changes.

Previous model-based work suggests that ozone forcing is the major driver of recent stratospheric cooling (*10*, *34*). A similar result holds in PCM: Ozone changes account for 123% of the total linear change in T4 over 1950–1999 and for 82% of the T4 decrease during the satellite era (Figs. 1D and 2B). The corresponding contributions of greenhouse gas forcing to T4 changes are only 9 and 3%, respectively (*6*). In contrast, well-mixed greenhouse gases are the major contributor to PCM's tropospheric warming and explain 174% of the total change in T2 over 1950–1999 (Figs. 1F and 2C). The ozone component of T2 changes is small over this period (−6%) (*35*). In PCM, therefore, the main effect of well-mixed greenhouse gases on tropopause height is through warming the troposphere rather than cooling the stratosphere.

Several additional features are noteworthy. Anthropogenic sulfate aerosols decrease tropopause height, primarily by cooling the troposphere (Figs. 1F and 2C). In the model, sulfate aerosols cause only a small decrease in T4 (Figs. 1D and 2B). Solar irradiance changes over the 20th century warm both the troposphere and the stratosphere, with offsetting effects on tropopause height. The sign of the solar effect on p_{LRT} must therefore depend on the relative magnitudes of solar-induced stratospheric and tropospheric warming. The small rise in tropopause height in S (Fig. 1B) suggests that for solar forcing, tropospheric warming is more important.

A key assumption in many detection studies is that the sum of the individual climate responses to several different forcing mechanisms is equal to the response obtained when these forcings are varied simultaneously (*8*, *9*, *36*). This implies that there are no strong interactions between individual forcings. We tested this assumption for p_{LRT}, T4, and T2 by comparing ALL results with the sum of the individual responses to G, A, O, S, and V (SUM). ALL and SUM show very similar global mean changes (Fig. 1, B, D, and F). For the three variables considered here, the estimated linear changes in SUM are within 10% (*37*) of the corresponding ALL values (Fig. 2). For these global-scale changes, additivity is a reasonable assumption.

Fingerprint analysis. We next used a standard detection method (*38*, *39*) to determine whether a model-predicted spatial pattern of externally forced p_{LRT} changes can be identified in reanalysis data. Our detection method assumes that the searched-for signal (the fingerprint, $\vec{f}$) is well represented by the first empirical orthogonal function (EOF) of the ALL ensemble mean (*30*). We search for an increasing expression of $\vec{f}$ in the NCEP and ERA p_{LRT} data and estimate the detection time—the time at which $\vec{f}$ becomes consistently identifiable at a stipulated 5% significance level. The climate noise estimates required for assessing statistical significance are obtained from 300-year control runs performed with PCM and the ECHAM model of the Max-Planck Institute for Meteorology in Hamburg (*40*).

Detection times are computed both with and without the global mean component of tropopause height change (*30*). If the spatial mean is included, detection results can be dominated by large global-scale changes. Removing the spatial mean focuses attention on smaller-scale model-data pattern similarities and provides a more stringent test of model performance.

We first describe the patterns of tropopause height change in PCM and reanalyses. Maps of linear p_{LRT} trends over 1979–1999 are similar in NCEP and PCM (Fig. 3, A and C). Both show spatially coherent increases in tropopause height (negative trends in p_{LRT}), with the smallest changes in the tropics and the largest increases toward the poles, particularly in the Southern Hemisphere (*6*). Tropopause height changes in ERA (Fig. 3B) are less coherent than

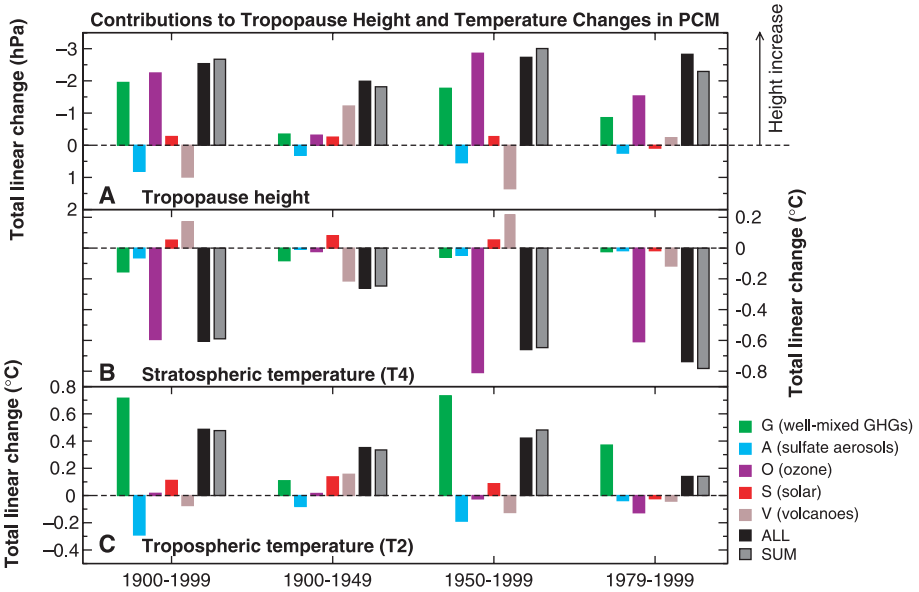

Fig. 2. Total linear changes (*32*) in global mean, monthly mean tropopause height (**A**), stratospheric temperature (**B**), and tropospheric temperature (**C**) in PCM experiments with individual forcings (G, A, O, S, and V) and combined natural and anthropogenic forcings (ALL). Linear changes are computed over four different time intervals using the (unfiltered) ensemble-mean data from Fig. 1. For each time period, anomalies were defined relative to climatological monthly means computed over 1900–1999. SUM denotes the sum of the linear changes in G, A, O, S, and V.

in NCEP or PCM, with slight decreases in height in the tropics. This largely reflects the shorter record length of ERA, which ends at a time when Pinatubo decreased tropopause height (Fig. 1, A and B). The ALL "mean included" p_{LRT} fingerprint is similar to the PCM and NCEP linear trend patterns, with uniform sign, largest loadings at high latitudes in the Southern Hemisphere, and strong zonal structure (Fig. 3D). Removal of the spatial means emphasizes the strong equator-to-pole gradients and hemispheric asymmetry of the fingerprint (Fig. 3E).

When our detection method is applied with spatial means included, the ALL tropopause height fingerprint is consistently identifiable in both reanalyses (fig. S1). Although ERA tropopause height increases are less coherent than in NCEP and are visually less similar to the ALL fingerprint, $\vec{f}$ is still readily detectable. In all four cases considered (*41*), fingerprint detection occurs in 1988, only 10 years after the start of our analysis period (1979). With our strategy, 1988 is the earliest time at which detection can be achieved.

The removal of spatial means still yields an identifiable fingerprint, but only in NCEP. This positive result arises from model-data similarities in the equator-to-pole gradient and the hemispheric asymmetry of tropopause height changes (Fig. 3, A and E). Detection of $\vec{f}$ in NCEP data occurs in 1995 (fig. S1), 7 years later than in the "mean included" case and after the end of the ERA record. This suggests that the ERA record is simply too short to achieve positive detection of subglobal features of the predicted tropopause height changes.

Conclusions. Our results are relevant to the issue of whether the "real-world" troposphere has warmed during the satellite era. PCM provides both direct and indirect evidence in support of a warming troposphere. The direct evidence is that in the ALL experiment, the troposphere warms by 0.07°C/decade over 1979–1999 (*30*). This warming is predominantly due to increases in well-mixed greenhouse gases (Fig. 2C). We have previously shown (*30*) that the T2 fingerprint estimated from ALL is identifiable in a satellite data set with a warming troposphere (*27*) but not in a satellite data set with little overall tropospheric temperature change (*28*).

The second (and more indirect) line of evidence relies on the relation between changes in tropopause height and changes in tropospheric temperature. Our detection results show consistency between the patterns of tropopause height increase in ALL and reanalyses. The PCM individual forcing experiments help to identify the main drivers of this change. Over 1979–1999, roughly 30% of the increase in tropopause height in ALL is explained by greenhouse gas–induced warming of the troposphere (Fig. 2A). Anthropogenically driven tropospheric warming is therefore an important factor in explaining modeled changes in tropopause height. Without this tropospheric warming effect in the model, simulated height changes would be markedly reduced, and the correspondence that we find between modeled and observed Δp_{LRT} would be substantially degraded. The inference is that human-induced tropospheric warming may also be an important driver of observed increases in tropopause height. Both the direct and indirect lines of evidence support the contention that the troposphere has warmed during the satellite era.

We have shown that both stratospheric cooling and tropospheric warming lead to increases in tropopause height. However, the relative importance of these two factors is uncertain. In the NCEP reanalysis, which has documented errors in stratospheric temperature (*31*), tropopause height increases even though the troposphere cools. In ERA (*22*) and PCM, the troposphere warms, and both stratospheric cooling and tropospheric warming contribute to tropopause height increases. Clarification of the relative roles of T2 and T4 changes in recent tropopause height increases is clearly required. This may be facilitated by second-generation reanalyses (such as the recently completed ERA-40 reanalysis), by further study of radiosonde-based temperature soundings, and by high-resolution measurements of the tropopause from Global Positioning System (GPS) data (*42*).

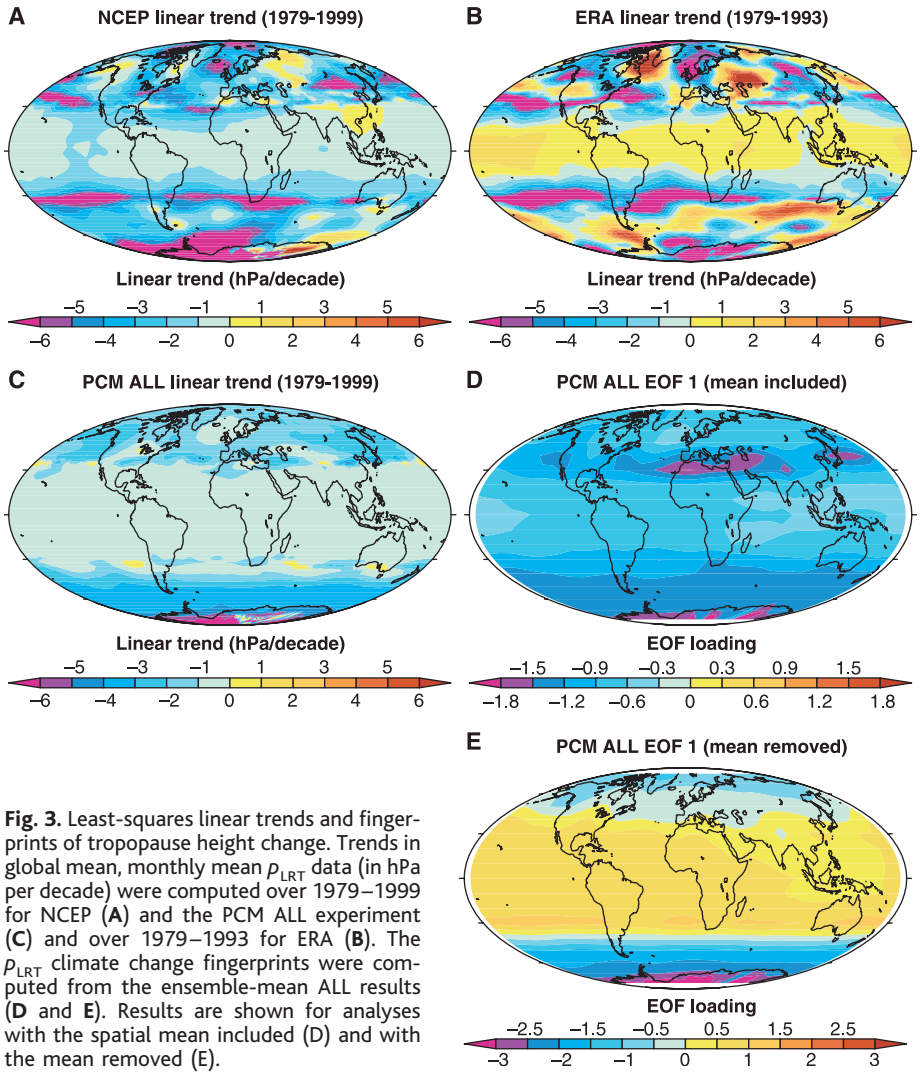

Fig. 3. Least-squares linear trends and fingerprints of tropopause height change. Trends in global mean, monthly mean p_{LRT} data (in hPa per decade) were computed over 1979–1999 for NCEP (**A**) and the PCM ALL experiment (**C**) and over 1979–1993 for ERA (**B**). The p_{LRT} climate change fingerprints were computed from the ensemble-mean ALL results (**D** and **E**). Results are shown for analyses with the spatial mean included (D) and with the mean removed (E).

References and Notes

1. K. P. Hoinka, *Mon. Weath. Rev.* **126**, 3303 (1998).
2. D. J. Seidel, R. J. Ross, J. K. Angell, G. C. Reid, *J. Geophys. Res.* **106**, 7857 (2001).
3. E. J. Highwood, B. J. Hoskins, *Q. J. R. Meteorol. Soc.* **124**, 1579 (1998).
4. E. J. Highwood, B. J. Hoskins, P. Berrisford, *Q. J. R. Meteorol. Soc.* **126**, 1515 (2000).
5. W. J. Randel, F. Wu, D. J. Gaffen, *J. Geophys. Res.* **105**, 15509 (2000).
6. B. D. Santer *et al.*, *J. Geophys. Res.* **108**, 4002 (2003) (DOI 10.1029/2002JD002258).
7. R. Sausen, B. D. Santer, *Meteorol. Zeit.* **12**, 131 (2003).
8. B. D. Santer *et al.*, *Nature* **382**, 39 (1996).
9. S. F. B. Tett, J. F. B. Mitchell, D. E. Parker, M. R. Allen, *Science* **274**, 1170 (1996).
10. V. Ramaswamy *et al.*, *Rev. Geophys.* **39**, 71 (2001).
11. J. E. Hansen *et al.*, *J. Geophys. Res.* **107**, 4347 (2002) (DOI 10.1029/2001JD001143).
12. W. M. Washington *et al.*, *Clim. Dyn.* **16**, 755 (2000).
13. J. T. Kiehl, T. L. Schneider, R. W. Portmann, S. Solomon, *J. Geophys. Res.* **104**, 31239 (1999).

14. A. Dai, T. M. L. Wigley, B. A. Boville, J. T. Kiehl, L. E. Buja, *J. Clim.* **14**, 485 (2001).
15. D. V. Hoyt, K. H. Schatten, *J. Geophys. Res.* **98**, 18895 (1993).
16. G. A. Meehl, W. M. Washington, T. M. L. Wigley, J. M. Arblaster, A. Dai, *J. Clim.* **16**, 426 (2003).
17. C. Ammann, G. A. Meehl, W. M. Washington, C. S. Zender, *Geophys. Res. Lett.* **30**, 1657 (2003) (DOI 10.1029/2003GL016875).
18. The G, A, and O forcings in the PCM experiments are identical to those used in integrations performed with the NCAR Climate System Model (*13*, *14*). Total solar irradiance changes were prescribed according to Hoyt and Schatten (*15*) and updated as in (*16*), with no wavelength dependence of the forcing. Volcanic forcing was based on estimates of total sulfate loading and a simplified model of aerosol distribution and decay (*17*).
19. E. Kalnay *et al.*, *Bull. Am. Meteorol. Soc.* **77**, 437 (1996).
20. J. K. Gibson *et al.*, *ECMWF Re-Analysis Project Reports Series 1* (European Centre for Medium-Range Weather Forecasts, Reading, UK, 1997), 66 pp.
21. S. Pawson, M. Fiorino, *Clim. Dyn.* **15**, 241 (1999).
22. B. D. Santer *et al.*, *J. Geophys. Res.* **104**, 6305 (1999).
23. World Meteorological Organization (WMO), *Meteorology—A Three-Dimensional Science: Second Session of the Commission for Aerology* [WMO Bulletin IV(4), WMO, Geneva, 1957], pp. 134–138.
24. T. Reichler, M. Dameris, R. Sausen, D. Nodorp, *A Global Climatology of the Tropopause Height Based on ECMWF Analyses* (Institut für Physik der Atmosphäre, Report 57, Deutsche Forschungsanstalt für Luft und Raumfahrt, Wessling, Germany, 1996).
25. We estimate p_{LRT} from reanalysis and model data by interpolation of the lapse rate in a p^{κ} coordinate system, where p denotes pressure, $\kappa = R/c_p$, and R and c_p are the gas constant for dry air and the specific heat capacity of dry air at constant pressure (*24*). The algorithm identifies the threshold model level at which the lapse rate falls below 2°C/km and then remains less than this critical value for a specified vertical distance (*23*). The exact pressure at which the lapse rate attains the critical value is determined by linear interpolation of lapse rates in the layers immediately above and below the threshold level. This definition of tropopause height is robust under most conditions. Exceptions include situations where the atmosphere is relatively isothermal or where multiple stable layers are present (*24*). To avoid unrealistically high or low p_{LRT} values, search limits are restricted to pressure levels between roughly 550 and 75 hPa. Decadal-scale trends in p_{LRT} are relatively insensitive to the temporal resolution of the input temperature data (*3*, *6*).
26. The NCEP p_{LRT} calculation performed here used monthly mean temperature data at 17 model pressure levels. A similar calculation used the 6-hourly temperature data available at 28 model sigma levels, with higher resolution in the vicinity of the tropical tropopause (*6*).
27. C. A. Mears, M. C. Schabel, F. W. Wentz, *J. Clim.*, in press.
28. J. R. Christy, R. W. Spencer, W. D. Braswell, *J. Atmos. Ocean. Tech.* **17**, 1153 (2000).
29. The radiative emissions contributing to the T4 and T2 measurements peak at roughly 74 and 595 hPa, respectively. In the tropics, emissions from the troposphere make a substantial contribution to estimated T4 temperatures.
30. B. D. Santer *et al.*, *Science* **300**, 1280 (2003).
31. The total linear change in T4 in NCEP is −1.65°C over 1979–1999 (*32*). This is considerably larger than the simulated T4 change of −0.73°C in ALL or the estimated observed MSU T4 changes of −0.93°C (*27*) and −1.07°C (*28*). NCEP's excessive stratospheric cooling is due to biases in both the satellite-derived temperature retrievals and the assimilated radiosonde data (*6*, *21*). Because T2 receives a small (roughly 10% globally) contribution from the stratosphere, any error in NCEP's T4 trends will propagate into ΔT2. This partly explains why NCEP's troposphere cools markedly over 1979–1999, with a total linear change in T2 of −0.22°C.
32. The total linear change is defined as $b \times n$, where b is the slope parameter of the linear trend (in hPa per month or °C per month) fitted by the standard least-squares method over a specified period of n months.
33. For forcing component x, this is calculated as $(x/y) \times 100$, where x is the total linear change in p_{LRT} over a stipulated time interval (due to x) and y is the linear change in p_{LRT} (over the same interval) due to ALL. This definition is not applicable if the linear change in ALL is close to zero, a situation that never arises here.
34. V. Ramaswamy, M. D. Schwarzkopf, W. Randel, *Nature* **382**, 616 (1996).
35. Because the O experiment does not separate tropospheric and stratospheric ozone changes, we cannot quantify their individual contributions to overall changes in p_{LRT}. Historical increases in tropospheric ozone are expected to warm T2, thereby increasing tropopause height. Such warming is not evident in the O integration (Fig. 2C) because of the cooling effect of stratospheric ozone depletion on the upper troposphere. Figure 2 indicates that in PCM, ozone-induced increases in tropopause height arise primarily through stratospheric ozone depletion and the resultant cooling of T4, not through tropospheric ozone changes.
36. P. A. Stott *et al.*, *Science* **290**, 2133 (2000).
37. Linear changes in tropopause height over 1979–1999 are the sole exception: SUM results are 19% smaller than in ALL. This difference is largely attributable to noise differences. SUM is a linear combination of five climate responses plus five different (ensemble-averaged) noise estimates, and must therefore be noisier than ALL. ALL versus SUM noise differences are likely to have the greatest impact on trends calculated over relatively short periods.
38. K. Hasselmann, in *Meteorology of Tropical Oceans*, D. B. Shaw, Ed. (Royal Meteorological Society of London, London, UK, 1979), pp. 251–259.
39. B. D. Santer *et al.*, *J. Geophys. Res.* **100**, 10693 (1995).
40. E. Roeckner, L. Bengtsson, J. Feichter, J. Lelieveld, H. Rodhe, *J. Clim.* **12**, 3004 (1999).
41. Two reanalyses (NCEP and ERA) combined with two noise data sets for calculation of natural variability statistics (PCM and ECHAM) yields four nonoptimized detection time estimates.
42. W. J. Randel, F. Wu, W. R. Rios, *J. Geophys. Res.* **108**, 4024 (2003) (DOI 10.1029/2002JD002595).

43. Work at Lawrence Livermore National Laboratory was performed under the auspices of the U.S. Department of Energy (DOE), Environmental Sciences Division, contract W-7405-ENG-48. T.M.L.W. was supported by the National Oceanic and Atmospheric Administration Office of Global Programs (Climate Change Data and Detection) grant no. NA87GP0105 and by DOE grant no. DE-FG02-98ER62601. A portion of this study was supported by the DOE Office of Biological and Environmental Research, as part of its Climate Change Prediction Program. The MSU weighting functions were provided by J. Christy (Univ. of Alabama in Huntsville). E. Roeckner (Max-Planck Institut für Meteorologie, Hamburg, Germany) supplied ECHAM control run data. Review comments from B. Hoskins and S. Pawson substantially improved the manuscript. We also thank R. Anthes, W. Randel, and J. Bates for bringing GPS-based monitoring of tropopause height to our attention.

Supporting Online Material

www.sciencemag.org/cgi/content/full/301/5632/479/DC1
SOM Text
Fig. S1

4 March 2003; accepted 30 May 2003

Dense Packing and Symmetry in Small Clusters of Microspheres

Vinothan N. Manoharan,[1] Mark T. Elsesser,[1] David J. Pine[1,2]*

When small numbers of colloidal microspheres are attached to the surfaces of liquid emulsion droplets, removing fluid from the droplets leads to packings of spheres that minimize the second moment of the mass distribution. The structures of the packings range from sphere doublets, triangles, and tetrahedra to exotic polyhedra not found in infinite lattice packings, molecules, or minimum–potential energy clusters. The emulsion system presents a route to produce new colloidal structures and a means to study how different physical constraints affect symmetry in small parcels of matter.

What defines an optimal packing of a set of n identical spheres? Although centuries old, this question remains both pertinent and pervasive in mathematics and science (*1*). For packings of an infinite number of spheres, the obvious measure of optimality is the bulk density. As Kepler conjectured and Hales proved (*2*, *3*), the optimal infinite packing is the face-centered cubic (fcc) arrangement, which maximizes the density or, equivalently, minimizes the volume per sphere. But for a finite group of spheres there is no compelling definition of density, and optimality in finite sphere packings can be defined by the minimization of any physically reasonable variable, such as potential energy or surface area, for example. Different minimization criteria can lead to dramatically different sequences of packings (*4*), with symmetries that are rarely consistent with that of an infinite (bulk) packing.

In nature, differences in symmetry between finite and bulk packings manifest themselves in a variety of phenomena. The interactions between atoms or particles in many systems, including metals, noble gases, and colloids, are nearly spherically isotropic, and the equilibrium structures at high density are fcc, a consequence of Kepler's conjecture. But finite packings of such particles, as found in isolated clusters, complexes, or local arrangements of bulk phases, frequently

[1]Department of Chemical Engineering, [2]Department of Materials, University of California, Santa Barbara, CA 93106, USA.

*To whom correspondence should be addressed. E-mail: pine@mrl.ucsb.edu